

# Formation dynamics in geostationary ring

Sofya Spiridonova<sup>1</sup>

Received: 2 September 2015 / Revised: 22 March 2016 / Accepted: 5 April 2016 /  
Published online: 10 May 2016  
© Springer Science+Business Media Dordrecht 2016

**Abstract** A relative motion model for a satellite formation composed of two Earth-orbiting spacecraft located in the geostationary ring is developed taking into account major gravitational and non-gravitational forces. A previously existing model featuring perturbation due to  $J_2$  is enhanced by the perturbations due to solar radiation pressure arising from unequal area-to-mass ratios, as well as the secular and long-periodic gravitational perturbations due to the Sun and the Moon. The extended relative motion model is validated using several typical formation geometries against a reference generated by numerical integration of the absolute orbits of the two spacecraft. The results of this work can find application in future on-orbit servicing and formation flying missions in near-geostationary orbit.

**Keywords** Relative motion · Solar radiation pressure (SRP) · Third-body gravitational perturbations · Geostationary orbit · Formation flying · On-orbit servicing (OOS) · Relative orbital elements (ROEs)

## 1 Introduction

As the market of satellite communication services is growing continuously, there is an ever-increasing interest in On-Orbit Servicing (OOS) and Space Situational Awareness (SSA) in near-geostationary orbit (GEO). A number of Phase A/B satellite mission studies have been conducted in the last decade (Caswell et al. 2006; Kaiser et al. 2008), which demonstrates strong demand as well as technological readiness for OOS in GEO. Potential applications of a geostationary OOS satellite include propellant supply for Client spacecraft life extension, provision of Attitude and Orbit Control (AOC) in case of Client AOC system malfunction, recovery of a satellite launched into an incorrect orbit, and last but not least, active removal

---

**Electronic supplementary material** The online version of this article (doi:[10.1007/s10569-016-9693-0](https://doi.org/10.1007/s10569-016-9693-0)) contains supplementary material, which is available to authorized users.

---

✉ Sofya Spiridonova  
sofya.spiridonova@dlr.de

<sup>1</sup> DLR/GSOC, Münchener Str. 20, 82234 Weßling, Germany

of space debris and de-orbiting of old uncooperative satellites. These considerations call for an in-depth investigation of the dynamics of the relative motion of two spacecraft in near-geostationary orbit.

A Relative Motion Model (RMM) was developed in [D'Amico \(2010\)](#) addressing secular perturbations due to the oblateness of the Earth as well as the differential air drag. This RMM has been employed at the German Space Operations Center (GSOC) in various Low-Earth Orbit (LEO) formation-flying experiments, ([D'Amico et al. 2012](#); [Gaias et al. 2014](#); [D'Amico et al. 2013](#)). It also forms the basis of the TanDEM-X Autonomous Formation Flying system ([Ardaens et al. 2011, 2013](#)). The goal of the present research is to extend the available RMM including perturbations that might be secondary in LEO but play a significant role at GEO altitude, such as the Solar Radiation Pressure (SRP) and the third-body gravitational pull. Due to the much longer revolution period in GEO as compared to LEO, all the OOS and formation flying activities, such as a spiral far- or mid-range approach, or an inspection fly-around, have a timely duration approximately 15 times longer than a corresponding activity in LEO, bringing into foreground certain secular and long-periodic perturbations.

The effects of SRP are particularly important for communication satellites equipped with large solar arrays. The topic of SRP affecting *absolute* orbits of single satellites has been discussed often in literature, ([Bryant 1961](#); [Kozai 1963](#); [Aksnes 1976](#)). As to the *relative* orbit, the key factor driving the differential SRP is the difference in area-to-mass ratio of the two spacecraft. If the objective is to provide on-orbit services to various Client spacecraft within a wide range of area-to-mass ratios, SRP becomes an important factor in approach trajectory design and relative orbit prediction. In present work, a simple model for inertial disturbing relative acceleration under the assumption of constant spacecraft cross-sectional areas proves sufficient to account for major SRP-related effects.

In near-geostationary orbit and with relatively large separation in the normal and radial directions as it can be, for instance, in the beginning of a rendezvous phase, third-body gravitational perturbations of the Sun and the Moon are no longer negligible. Third-body perturbations of *absolute* orbits have been studied intensively in the second half of the last century. Among the major contributions are: the developments in [Kaula \(1962\)](#), analogous to the well-known Linear Perturbation Theory for gravitational perturbations of non-spherical Earth; the formalization of [Kozai \(1973\)](#), where the disturbing function is represented in terms of the polar coordinates of the disturbing body and the Keplerian elements of the satellite; the theory of [Giacaglia \(1974\)](#), where the perturbations due to the Moon are developed in terms of its ecliptic elements; the double-averaged analytical model of [Prado \(2003\)](#), where the disturbing function is averaged over the satellites revolution period as well as the perturbing body's revolution period. The research on third-body perturbations in *relative* orbits, however, has been so far restricted primarily to numerical investigations, ([Wnuk and Golebiewska 2005](#)), and some analytical developments of relative perturbations based on the absolute double-averaged model of Prado. A simplified model of Prado was used in [Roscoe et al. \(2013\)](#), where the rates of the lunar perturbations in differential Keplerian elements were obtained as well as a transformation between the osculating elements and the lunar-averaged elements. In present research, the lunisolar secular and long-periodic gravitational perturbations of relative orbit were investigated using the formulations from [Kozai \(1973\)](#) for absolute orbits. Since the theory of Kozai delivers a single-averaged disturbing function, no transformation to mean lunar/solar orbital elements is necessary. Thus, the obtained perturbations depend on the actual position of the perturbing body and therefore give insight into the medium-term behavior of the satellite formation.

The ultimate result of this research is an extended relative motion model addressing relative dynamics of two spacecraft in near-geostationary orbit, which allows to predict the

evolution of the relative orbit from epoch  $t$  to epoch  $t + \Delta t$  taking into account SRP as well as third-body perturbations. The calculations require the Servicer’s absolute orbital elements obtained, for instance, through orbit determination using ground station tracking data, and the information on the relative orbital state at epoch  $t$ . Perturbations related to the Sun and the Moon depend as well on the geocentric position of the perturbing body. The absolute elements of the Client spacecraft are not required for the relative orbit prediction, and therefore this approach can be used in design of guidance profiles towards uncooperative targets as well as on-board a Servicer spacecraft for future OOS strategies with high level of autonomy.

The remaining of the paper is organized as follows. Section 2 recalls the relative motion model developed in D’Amico (2010), while Sect. 3 provides details on the extended RMM, including Sect. 3.1 dedicated to the differential SRP and Sect. 3.2 addressing third-body gravitational perturbations. Several initial formation geometries are selected in Sect. 4 covering a range of typical scenarios related to OOS and formation flying. These are used to validate the extended RMM with respect to a reference generated by numerical integration of two absolute orbits under full force model.

## 2 Preliminaries

### 2.1 Relative orbital elements

The relative motion of two close spacecraft in Low Earth Orbit (LEO) was characterized in D’Amico (2010) in terms of the following set of Relative Orbital Elements (ROEs)

$$\delta\alpha = \begin{pmatrix} \delta a \\ \delta\lambda \\ \delta e_x \\ \delta e_y \\ \delta i_x \\ \delta i_y \end{pmatrix} = \begin{pmatrix} (a_d - a) / a \\ (u_d - u) + (\Omega_d - \Omega) \cos i \\ e_{x,d} - e_x \\ e_{y,d} - e_y \\ i_d - i \\ (\Omega_d - \Omega) \sin i \end{pmatrix}, \tag{1}$$

where the non-singular elements

$$\begin{aligned} \kappa &= (a, u, e_x, e_y, i, \Omega)^T \\ &= (a, \omega + M, e \cos \omega, e \sin \omega, i, \Omega)^T \end{aligned} \tag{2}$$

parametrize the absolute orbit of a single satellite. Here  $a, e, i, \Omega, \omega, M$  are the classical Keplerian elements. The subscript  $d$  refers to the deputy satellite, while the orbital elements without a subscript denote the elements of the chief satellite.

The general concept of the ROEs above was inherited from the previous studies on safe colocation of geostationary satellites (Härting et al. 1988; Eckstein et al. 1989), and adapted to formation flight in D’Amico (2010) to parameterize the relative motion of the deputy satellite with respect to the chief satellite. With OOS applications being the baseline scenario of the present paper, the Client satellite is considered to be the chief satellite, while the motion of the Servicer has to be characterized with respect to the Client. On the other hand, the orbit of the Servicer will probably be known with better accuracy than the orbit of a possibly

uncooperative Client. Therefore, a slightly different definition of ROEs will be used in the remaining of the paper:

$$\widetilde{\delta\alpha} = \begin{pmatrix} \widetilde{\delta a} \\ \widetilde{\delta\lambda} \\ \delta e_x \\ \delta e_y \\ \widetilde{\delta i_x} \\ \widetilde{\delta i_y} \end{pmatrix} = \begin{pmatrix} (a_s - a_c) / a_s \\ (u_s - u_c) + (\Omega_s - \Omega_c) \cos i_s \\ e_{x,s} - e_{x,c} \\ e_{y,s} - e_{y,c} \\ i_s - i_c \\ (\Omega_s - \Omega_c) \sin i_s \end{pmatrix}, \tag{3}$$

where the subscripts *s* and *c* refer to the Servicer and the Client.

Compared to the original definition from **D’Amico (2010)**, the absolute elements of the chief (Client) satellite are substituted with the orbital elements of the deputy (Servicer) satellite in  $\delta a$ ,  $\delta\lambda$  and  $\delta i_y$  where they play a role of scaling factors. For instance, rewriting the definition from **D’Amico (2010)** using the subscripts *s* and *c* would give  $\delta a = (a_s - a_c) / a_c$ . Simple calculations show that

$$\widetilde{\delta a} = \delta a - \delta a \cdot \widetilde{\delta a} = \delta a + o(\delta a),$$

i.e., to the first order these definitions coincide. The same is true for the  $\delta\lambda$  and  $\delta i_y$ , namely

$$\widetilde{\delta\lambda} \approx \delta\lambda - \delta i_y \cdot \delta i_x = \delta\lambda + o(\delta\alpha),$$

and

$$\widetilde{\delta i_y} \approx \delta i_y + (\delta\lambda - \delta u) \cdot \delta i_x = \delta i_y + o(\delta\alpha).$$

Both the RMM developed in **D’Amico (2010)** and the extended RMM presented in this paper are linear in ROEs, and are only valid for near-circular orbits with  $\delta\alpha \ll 1$ . The error introduced by deviations in the definitions of ROEs is, however, of second order, and therefore, the modified ROEs are subject to the same first-order dynamics as characterized in **D’Amico (2010)**. In the following, the symbol of tilde in  $\widetilde{\delta\{\cdot\}}$  will be omitted.

Vectors  $\delta e = (\delta e_x, \delta e_y)^T$  and  $\delta i = (\delta i_x, \delta i_y)^T$  are called the relative eccentricity and the relative inclination vectors with magnitudes denoted by  $\delta e$  and  $\delta i$ , respectively.

Multiplied by the semi-major axis, ROEs allow a convenient representation of the ideal relative in-plane and out-of-plane motion. Namely, under the assumptions of near-circular orbits and  $\delta\alpha \ll 1$ , the relative motion is bounded, if the offset in the semi-major axes  $a\delta a$  is zero. In the orbital plane, the Servicer circumscribes with respect to the Client an ellipse with semi-major axis  $2a\delta e$  in along-track direction and semi-minor axis  $a\delta e$  in radial direction, whereas the amplitude of the oscillation in the direction orthogonal to the orbital plane is equal to  $a\delta i$  (see, for instance, Fig. 2.2 in **D’Amico 2010**). The average relative offsets in the along-track and radial directions are equal to  $a\delta\lambda$  and  $a\delta a$ , respectively.

Along with the definition in Eq. (3) a set of differences

$$\Delta\kappa = \begin{pmatrix} \Delta a \\ \Delta u \\ \Delta e_x \\ \Delta e_y \\ \Delta i \\ \Delta\Omega \end{pmatrix} = \begin{pmatrix} a_s - a_c \\ u_s - u_c \\ e_{x,s} - e_{x,c} \\ e_{y,s} - e_{y,c} \\ i_s - i_c \\ \Omega_s - \Omega_c \end{pmatrix} \tag{4}$$

is used in auxiliary computations. The relations between  $\delta\alpha$  and  $\Delta\kappa$  are straightforward

$$\begin{aligned} \delta a &= \Delta a/a_s & \delta\lambda &= \Delta u + \Delta\Omega \cos i_s \\ \delta e_x &= \Delta e_x & \delta e_y &= \Delta e_y \\ \delta i_x &= \Delta i & \delta i_y &= \Delta\Omega \sin i_s. \end{aligned} \tag{5}$$

All the absolute orbital elements that appear in the following refer to those of the Servicer satellite, therefore the subscript  $s$  is dropped.

### 2.2 Unperturbed relative motion and the Earth oblateness terms

Under the assumptions of the Hill-Clohesy-Wiltshire (HCW) equations governing unperturbed relative motion (Clohesy and Wiltshire 1960), the only relative element changing with time is the relative mean longitude  $a\delta\lambda$ . Namely, if the semi-major axis offset  $a\delta a$  is not zero, the Servicer is drifting with respect to the Client with a rate of  $-3\pi a\delta a$  per revolution. At the same time, main secular perturbations of the almost-bounded relative motion resulting from the Earth equatorial bulge can be summarized as a rotation of the relative eccentricity vector  $a\delta e$ , and in case  $\delta i_x \neq 0$ , a vertical drift of the relative inclination vector  $a\delta i$  and an additional drift of the relative mean argument of longitude  $a\delta\lambda$ .

A detailed analysis of the unperturbed motion and the perturbations due to  $J_2$  can be found in D’Amico (2010). Motivated by the future Autonomous Vision Approach Navigation and Target Identification (AVANTI) experiment (Gaias et al. 2014), this model was revisited in Gaias et al. (2015) where perturbations arising from non-zero  $a\delta a$  were derived and included into the model. The final form of the available relative motion model as formulated in Gaias et al. (2015) is recalled below:

$$a\delta\alpha(t + \Delta t) = (\Phi_{\text{HCW}}(\kappa, \Delta t) + \Phi_{J_2}(\kappa, \Delta t)) \cdot a\delta\alpha(t), \tag{6}$$

where the sum of the state transition matrices

$$\Phi_{\text{HCW}} = \begin{pmatrix} 1 & 0 & 0 & 0 & 0 & 0 \\ -\frac{3}{2}n\Delta t & 1 & 0 & 0 & 0 & 0 \\ 0 & 0 & 1 & 0 & 0 & 0 \\ 0 & 0 & 0 & 1 & 0 & 0 \\ 0 & 0 & 0 & 0 & 1 & 0 \\ 0 & 0 & 0 & 0 & 0 & 1 \end{pmatrix}$$

and

$$\Phi_{J_2} = n\Delta t \begin{pmatrix} 0 & 0 & 0 & 0 & 0 & 0 \\ -\frac{21}{4}\gamma H(\eta + 1) & 0 & 0 & 0 & -\frac{3}{2}\gamma \sin 2i(3\eta + 4) & 0 \\ 0 & 0 & 0 & -\varphi' & 0 & 0 \\ 0 & 0 & \varphi' & 0 & 0 & 0 \\ 0 & 0 & 0 & 0 & 0 & 0 \\ -\frac{21}{4}\gamma \sin 2i & 0 & 0 & 0 & 3\gamma \sin^2 i & 0 \end{pmatrix},$$

describes the evolution of ROEs in the time span of  $\Delta t$  under the influence of the oblate Earth. Here,  $\eta = \sqrt{1 - e^2}$ ,  $H = 3 \cos^2 i - 1$ ,  $\varphi' = \frac{3}{2}\gamma (5 \cos^2 i - 1)$ ,  $\gamma = \frac{J_2}{2} \left(\frac{R_E}{a}\right)^2 \frac{1}{(1-e^2)^2}$ ,  $J_2 \approx 1.082 \cdot 10^{-3}$ , while  $n$  is the Servicer mean motion,  $\kappa$  are the Servicer non-singular orbital elements from Eq. (2), and  $R_E$  is the Earth equatorial radius.

For the sake of completeness, the following linear mapping obtained in Section 2.2.1 of D’Amico (2010) based on the equivalence between the ROEs and the integration constants

in the HCW equations is recalled below providing a transformation between the ROEs and the components of the relative position and velocity vectors in the orbital frame:

$$\begin{pmatrix} \delta \mathbf{r}_{RTN} \\ \delta \mathbf{v}_{RTN} \end{pmatrix} = \mathbf{A} \cdot a\delta\boldsymbol{\alpha}, \tag{7}$$

where

$$\mathbf{A} = \begin{pmatrix} 1 & 0 & -\cos u & -\sin u & 0 & 0 \\ 0 & 1 & 2 \sin u & -2 \cos u & 0 & 0 \\ 0 & 0 & 0 & 0 & \sin u & -\cos u \\ 0 & 0 & n \sin u & -n \cos u & 0 & 0 \\ -1.5n & 0 & 2n \cos u & 2n \sin u & 0 & 0 \\ 0 & 0 & 0 & 0 & n \cos u & n \sin u \end{pmatrix},$$

and the orbital RTN reference frame is formed by the coordinate axes pointing in zenith direction (radial), along-track in-flight direction (tangential), and the direction orthogonal to the orbital plane (normal), with the origin of the reference frame located at the Client satellite.

### 3 Extended relative motion model

The complete extended model of relative motion in near-geostationary orbit can be formulated as

$$\begin{aligned} a\delta\boldsymbol{\alpha}(t + \Delta t) &= (\boldsymbol{\Phi}_{HCW}(\boldsymbol{\kappa}, \Delta t) + \boldsymbol{\Phi}_{J_2}(\boldsymbol{\kappa}, \Delta t)) \cdot a\delta\boldsymbol{\alpha}(t) \\ &+ a\Delta\delta\boldsymbol{\alpha}_{SRP}(\boldsymbol{\kappa}, \delta\boldsymbol{\alpha}(t), \mathbf{r}_{Sun}, \Delta t) \\ &+ a\Delta\delta\boldsymbol{\alpha}_{Sun}(\boldsymbol{\kappa}, \delta\boldsymbol{\alpha}(t), \mathbf{r}_{Sun}, \Delta t) \\ &+ a\Delta\delta\boldsymbol{\alpha}_{Moon}(\boldsymbol{\kappa}, \delta\boldsymbol{\alpha}(t), \mathbf{r}_{Moon}, \Delta t). \end{aligned} \tag{8}$$

The changes in ROEs occurred during  $\Delta t$  under the influence of SRP and third bodies are denoted in Eq. (8) by  $a\Delta\delta\boldsymbol{\alpha}_{SRP}$  and  $a\Delta\delta\boldsymbol{\alpha}_{Sun/Moon}$ , respectively. The following subsections are dedicated to the derivation of these components, which constitutes the main result of this paper.

#### 3.1 Differential SRP perturbations

To take SRP into account the simplest model (Montenbruck and Gill 2000) is used according to which the perturbing acceleration is

$$\delta\ddot{\mathbf{r}} = -P_{\odot}C_R \frac{A_R \mathbf{r}_{\odot}}{m r_{\odot}^3} \text{AU}^2, \tag{9}$$

where  $P_{\odot} \approx 4.56 \times 10^{-6} \text{Nm}^{-2}$  is the constant of the solar radiation pressure,  $C_R$  accounts for the mean reflectivity of the surface,  $A_R$  is the spacecraft cross-sectional area assumed constant, Astronomical Unit  $\text{AU} \approx 1.4960 \times 10^8 \text{ km}$ ,  $m$  is the mass of the spacecraft, and  $\mathbf{r}_{\odot}$  is the relative position vector of the spacecraft with respect to the Sun. The symbol  $\delta$  in front of  $\ddot{\mathbf{r}}$  implies here that this acceleration is of perturbational character, yet *absolute*.

Given the large distance to the Sun as compared to the distance between the satellites it suffices to assume that the distance to the Sun and the unit direction-to-the-Sun vector are the same for both spacecraft. In this way, the differential SRP coefficient

$$\text{DR} = C_{R_s} \frac{A_{R_s}}{m_s} - C_{R_c} \frac{A_{R_c}}{m_c}$$

is the only parameter of influence, and the *relative* perturbing acceleration is approximated as

$$\Delta\delta\ddot{\mathbf{r}} = -P_{\odot}DR \frac{\mathbf{r}_{\odot}}{r_{\odot}^3}AU^2. \tag{10}$$

The corresponding increments of the relative velocity and position in the Earth-centered inertial reference system (ECI) are

$$\Delta\delta\mathbf{v}_{\text{ECI}} \approx \Delta\delta\dot{\mathbf{r}} \cdot \Delta t, \quad \Delta\delta\mathbf{r}_{\text{ECI}} \approx \Delta\delta\ddot{\mathbf{r}} \cdot \frac{\Delta t^2}{2}.$$

The above vectors can be transformed to the RTN reference frame,

$$\Delta\delta\mathbf{v}_{\text{RTN}} = R_{\text{ECI2RTN}}\Delta\delta\mathbf{v}_{\text{ECI}}, \quad \Delta\delta\mathbf{r}_{\text{RTN}} = R_{\text{ECI2RTN}}\Delta\delta\mathbf{r}_{\text{ECI}},$$

where

$$R_{\text{ECI2RTN}} = \begin{pmatrix} \mathbf{e}_R^T \\ \mathbf{e}_T^T \\ \mathbf{e}_N^T \end{pmatrix}$$

and  $\mathbf{e}_R$ ,  $\mathbf{e}_T$  and  $\mathbf{e}_N$  are the unit vectors of the orbital coordinate frame expressed in the ECI frame.

Given the linear nature of the relation from Eq.(7), it allows to compute the perturbing component in ROEs from Eq.(8):

$$a\Delta\delta\boldsymbol{\alpha}_{\text{SRP}} = A^{-1} \begin{pmatrix} \Delta\delta\mathbf{r}_{\text{RTN}} \\ \Delta\delta\mathbf{v}_{\text{RTN}} \end{pmatrix}.$$

During the spring and autumn eclipse periods, satellites in near-geostationary orbit pass once per day through the Earth shadow. Shadow transitions are incorporated into the SRP model of the extended RMM based on the assumption that the eclipses occur simultaneously for the two satellites. A conical shadow model from [Montenbruck and Gill \(2000\)](#) is applied, where the perturbing relative acceleration  $\Delta\delta\ddot{\mathbf{r}}$  is scaled with the corresponding illumination factor provided by a dedicated shadow function.

### 3.2 Differential third-body perturbations

The following Lagrange equations apply for the perturbations in the non-singular absolute orbital elements  $\boldsymbol{\kappa}$  (e.g. [Ustinov 1967](#)).

$$\begin{aligned} \frac{d\delta a}{dt} &= \frac{2}{na} \frac{\partial R}{\partial u} \\ \frac{d\delta e_x}{dt} &= \frac{\eta}{na^2} \left( \frac{\partial R}{\partial e_y} + \frac{e_x}{1+\eta} \frac{\partial R}{\partial u} \right) + \frac{e_y \cot i}{na^2\eta} \frac{\partial R}{\partial i} \\ \frac{d\delta e_y}{dt} &= \frac{\eta}{na^2} \left( \frac{\partial R}{\partial e_x} - \frac{e_y}{1+\eta} \frac{\partial R}{\partial u} \right) - \frac{e_x \cot i}{na^2\eta} \frac{\partial R}{\partial i} \\ \frac{d\delta i}{dt} &= \frac{\cot i}{na^2\eta} \left( e_x \frac{\partial R}{\partial e_y} - e_y \frac{\partial R}{\partial e_x} + \frac{\partial R}{\partial u} \right) - \frac{\csc i}{na^2\eta} \frac{\partial R}{\partial \Omega} \\ \frac{d\delta \Omega}{dt} &= \frac{\csc i}{na^2\eta} \frac{\partial R}{\partial i} \\ \frac{d\delta u}{dt} &= -\frac{2}{na} \frac{\partial R}{\partial a} + \frac{\eta}{1+\eta} \frac{1}{na^2} \left( e_y \frac{\partial R}{\partial e_y} + e_x \frac{\partial R}{\partial e_x} \right) - \frac{\cot i}{na^2\eta} \frac{\partial R}{\partial i}, \end{aligned} \tag{11}$$

where  $\eta = \sqrt{1 - e_x^2 - e_y^2}$  and  $R$  is the so-called disturbing function or perturbing potential such that  $F = \frac{\mu}{2a} + R$ , where  $F$  is the total force function, i.e

$$F = V + R - T = \frac{\mu}{r} + R - \frac{v^2}{2} = \frac{\mu}{2a} + R,$$

$V$  and  $T$  being the undisturbed potential and the kinetic energy respectively.

In the above,  $\delta\{\cdot\}$  refers to the perturbations in the absolute orbital elements from Eq. (2), and not to the relative orbital elements from Eq. (3).

In [Kozai \(1973\)](#), the disturbing function for lunar and solar gravitational perturbations of absolute near-geostationary orbits was expressed as a function of the classical Keplerian elements of the satellite and the polar coordinates of the Sun and the Moon. To separate the secular and long-periodic terms from the short-periodic terms, the disturbing function was averaged in [Kozai \(1973\)](#) with respect to the mean anomaly of the satellite.

Re-writing the averaged disturbing function from [Kozai \(1973\)](#) in terms of the non-singular elements from Eq. (2) gives

$$\begin{aligned} R = n'^2 a^2 \left(\frac{a'}{r'}\right)^3 \beta \cdot \left\{ \frac{1}{16} \left( 3 \cos^2 \delta (2 - \sin^2 i) + 6 \sin^2 i \sin^2 \delta - 4 - 6 \sin i \sin 2\delta \right. \right. \\ \times \sin(\Omega - \alpha) + 3 \sin^2 i \cos^2 \delta \cos(2\Omega - 2\alpha) \Big) \left( 2 + 3e_x^2 + 3e_y^2 \right) + \frac{15}{8} \left( \cos^2 \delta \right. \\ \times \left[ \left( e_x^2 - e_y^2 \right) \cos(2\Omega - 2\alpha) - 2e_x e_y \sin(2\Omega - 2\alpha) \right] + \sin i \sin 2\delta \left[ \left( e_x^2 - e_y^2 \right) \right. \\ \times \sin(\Omega - \alpha) + 2e_x e_y \cos(\Omega - \alpha) \Big] \Big) - \frac{15}{32} \left( \frac{a}{a'} \right) \left( \frac{a'}{r'} \right) \left( 2 \cos \delta (5 \cos^2 \delta - 4) \right. \\ \times \left[ e_x \cos(\Omega - \alpha) - e_y \sin(\Omega - \alpha) \right] + 4 \sin i \sin \delta (5 \cos^2 \delta - 2) e_y - 5 \sin i \\ \times \sin 2\delta \cos \delta \left[ e_x \sin(2\Omega - 2\alpha) + e_y \cos(2\Omega - 2\alpha) \right] \Big) + \frac{3}{64} \left( \frac{a}{a'} \right)^2 \left( \frac{a'}{r'} \right)^2 \left( 35 \right. \\ \times \cos^4 \delta - 40 \cos^2 \delta + 8 - 10 \sin i \sin 2\delta (7 \cos^2 \delta - 4) \sin(\Omega - \alpha) \Big) - \frac{105}{128} \left( \frac{a}{a'} \right)^3 \\ \left. \times \left( \frac{a'}{r'} \right)^3 (21 \cos^4 \delta - 28 \cos^2 \delta + 8) \cos \delta \left( e_x \cos(\Omega - \alpha) - e_y \sin(\Omega - \alpha) \right) \right\}, \end{aligned}$$

where the motion of the perturbing body — the Sun or the Moon — is parametrized by the geocentric distance  $r'$ , right ascension  $\alpha$ , and declination  $\delta$ . These parameters can be found from the geocentric rectangular coordinates

$$\begin{aligned} x' &= r' \cos \delta \cos \alpha \\ y' &= r' \cos \delta \sin \alpha \\ z' &= r' \sin \delta. \end{aligned}$$



In the development of  $R$ , primed quantities  $n'$  and  $a'$  denote the mean motion and the semi-major axis of the perturbing body, while

$$\beta = \begin{cases} 1 & \text{for the Sun} \\ \frac{m'}{m + m'} & \text{for the Moon} \end{cases},$$

where  $m$  is the mass of the Earth and  $m'$  is the mass of the Moon.

According to the Lagrange equations in Eq. (11), the rates of the *absolute* perturbations are non-linear functions of the absolute orbital elements  $\kappa$ , which can be shortly written as

$$\delta \dot{\kappa} = F(\kappa). \tag{12}$$

Provided that  $F$  is differentiable at point  $\kappa \in \mathbb{R}^6$  and assuming that the separation between the satellites is small, we can approximate linearly the rates of the *differential* perturbations as

$$\Delta \delta \dot{\kappa} \approx J_F \cdot \Delta \kappa, \tag{13}$$

where  $J_F$  is the Jacobian matrix of the system of equations in Eq. (12), i.e.

$$J_F = \begin{pmatrix} \frac{\partial \delta \dot{a}}{\partial a} & \frac{\partial \delta \dot{a}}{\partial u} & \cdots & \frac{\partial \delta \dot{a}}{\partial \Omega} \\ \frac{\partial \delta \dot{u}}{\partial a} & \frac{\partial \delta \dot{u}}{\partial u} & \cdots & \frac{\partial \delta \dot{u}}{\partial \Omega} \\ \frac{\partial a}{\partial a} & \frac{\partial u}{\partial u} & \cdots & \frac{\partial \Omega}{\partial \Omega} \\ \vdots & \vdots & \ddots & \vdots \\ \frac{\partial \delta \dot{\Omega}}{\partial a} & \frac{\partial \delta \dot{\Omega}}{\partial u} & \cdots & \frac{\partial \delta \dot{\Omega}}{\partial \Omega} \end{pmatrix}.$$

Since the disturbing function  $R$  has been averaged over the satellite’s revolution period,  $\frac{\partial R}{\partial u} = 0$  and  $\delta \dot{a} = 0$ , the first line as well as the second column in  $J_F$  contain only zeros. Moreover,  $R$  being a polynomial in  $a$ , the entries in the first column of  $J_F$  are by factor  $O(a)$  smaller than the remaining non-zero terms.

Following Eq. (13), the Lagrange equations are differentiated to find the rates of the differential perturbations in  $u, e_x, e_y, i$  and  $\Omega$ :

$$\begin{aligned} \Delta \delta \dot{u} \approx & \left\{ -\frac{2}{na} \frac{\partial^2 R}{\partial a^2} + \frac{\eta}{1 + \eta} \frac{1}{na^2} \left( e_y \frac{\partial^2 R}{\partial a \partial e_y} + e_x \frac{\partial^2 R}{\partial a \partial e_x} \right) - \frac{\cot i}{na^2 \eta} \frac{\partial^2 R}{\partial a \partial i} + \frac{2}{na^2} \right. \\ & \times \left. \frac{\partial R}{\partial a} - \frac{2\eta}{1 + \eta} \frac{1}{na^3} \left( e_y \frac{\partial R}{\partial e_y} + e_x \frac{\partial R}{\partial e_x} \right) + \frac{2 \cot i}{na^3 \eta} \frac{\partial R}{\partial i} \right\} \cdot \Delta a + \left\{ -\frac{2}{na} \frac{\partial^2 R}{\partial a \partial e_x} \right. \\ & + \frac{\eta}{1 + \eta} \frac{1}{na^2} \left( e_y \frac{\partial^2 R}{\partial e_x \partial e_y} + e_x \frac{\partial^2 R}{\partial e_x^2} + \frac{\partial R}{\partial e_x} \right) - \frac{e_x}{\eta (1 + \eta)^2} \frac{1}{na^2} \left( e_y \frac{\partial R}{\partial e_y} + e_x \right. \\ & \times \left. \frac{\partial R}{\partial e_x} \right) - \frac{e_x \cot i}{\eta^3} \frac{\partial R}{na^2 \partial i} - \frac{\cot i}{na^2 \eta} \frac{\partial^2 R}{\partial e_x \partial i} \left. \right\} \cdot \Delta e_x + \left\{ -\frac{2}{na} \frac{\partial^2 R}{\partial a \partial e_y} + \frac{\eta}{1 + \eta} \frac{1}{na^2} \right. \\ & \times \left( e_x \frac{\partial^2 R}{\partial e_x \partial e_y} + e_y \frac{\partial^2 R}{\partial e_y^2} + \frac{\partial R}{\partial e_y} \right) - \frac{e_y}{\eta (1 + \eta)^2} \frac{1}{na^2} \left( e_y \frac{\partial R}{\partial e_y} + e_x \frac{\partial R}{\partial e_x} \right) \\ & \left. - \frac{e_y \cot i}{\eta^3} \frac{\partial R}{na^2 \partial i} - \frac{\cot i}{na^2 \eta} \frac{\partial^2 R}{\partial e_y \partial i} \right\} \cdot \Delta e_y + \left\{ -\frac{2}{na} \frac{\partial^2 R}{\partial a \partial i} + \frac{\eta}{1 + \eta} \frac{1}{na^2} \left( e_y \frac{\partial R}{\partial e_y \partial i} \right. \right. \end{aligned}$$

$$\begin{aligned}
 & + e_x \frac{\partial R}{\partial e_x \partial i} \Big) - \frac{\cot i}{na^2 \eta} \frac{\partial^2 R}{\partial i^2} + \frac{\csc^2 i}{na^2 \eta} \frac{\partial R}{\partial i} \Big\} \cdot \Delta i + \left\{ -\frac{2}{na} \frac{\partial^2 R}{\partial a \partial \Omega} + \frac{\eta}{1 + \eta} \frac{1}{na^2} \right. \\
 & \times \left. \left( e_y \frac{\partial^2 R}{\partial e_y \partial \Omega} + e_x \frac{\partial^2 R}{\partial e_x \partial \Omega} \right) - \frac{\cot i}{na^2 \eta} \frac{\partial^2 R}{\partial i \partial \Omega} \right\} \cdot \Delta \Omega \\
 \Delta \delta \dot{e}_x \approx & \left\{ \frac{\eta}{na^2} \frac{\partial^2 R}{\partial a \partial e_y} + \frac{e_y \cot i}{na^2 \eta} \frac{\partial^2 R}{\partial a \partial i} - \frac{2 d \delta e_x}{a dt} \right\} \Delta a + \left\{ -\frac{e_x}{na^2 \eta} \frac{\partial R}{\partial e_y} \right. \\
 & + \frac{\eta}{na^2} \frac{\partial^2 R}{\partial e_x \partial e_y} + \frac{e_x e_y \cot i}{na^2 \eta^3} \frac{\partial R}{\partial i} + \frac{e_y \cot i}{na^2 \eta} \frac{\partial^2 R}{\partial e_x \partial i} \Big\} \Delta e_x + \left\{ -\frac{e_y}{na^2 \eta} \frac{\partial R}{\partial e_y} \right. \\
 & + \frac{\eta}{na^2} \frac{\partial^2 R}{\partial e_y^2} + \frac{(1 - e_x^2) \cot i}{na^2 \eta^3} \frac{\partial R}{\partial i} + \frac{e_y \cot i}{na^2 \eta} \frac{\partial^2 R}{\partial e_y \partial i} \Big\} \Delta e_y + \left\{ \frac{\eta}{na^2} \frac{\partial^2 R}{\partial e_y \partial i} \right. \\
 & - \frac{e_y \csc^2 i}{na^2 \eta} \frac{\partial R}{\partial i} + \frac{e_y \cot i}{na^2 \eta} \frac{\partial^2 R}{\partial i^2} \Big\} \Delta i + \left\{ \frac{\eta}{na^2} \frac{\partial^2 R}{\partial e_y \partial \Omega} + \frac{e_y \cot i}{na^2 \eta} \frac{\partial^2 R}{\partial i \partial \Omega} \right\} \Delta \Omega \\
 \Delta \delta \dot{e}_y \approx & \left\{ \frac{\eta}{na^2} \frac{\partial^2 R}{\partial a \partial e_x} - \frac{e_x \cot i}{na^2 \eta} \frac{\partial^2 R}{\partial a \partial i} - \frac{2 d \delta e_y}{a dt} \right\} \Delta a + \left\{ -\frac{e_x}{na^2 \eta} \frac{\partial R}{\partial e_x} \right. \\
 & + \frac{\eta}{na^2} \frac{\partial^2 R}{\partial e_x^2} - \frac{(1 - e_y^2) \cot i}{na^2 \eta^3} \frac{\partial R}{\partial i} - \frac{e_x \cot i}{na^2 \eta} \frac{\partial^2 R}{\partial e_x \partial i} \Big\} \Delta e_x + \left\{ -\frac{e_y}{na^2 \eta} \frac{\partial R}{\partial e_x} \right. \\
 & + \frac{\eta}{na^2} \frac{\partial^2 R}{\partial e_x \partial e_y} - \frac{e_x e_y \cot i}{na^2 \eta^3} \frac{\partial R}{\partial i} - \frac{e_x \cot i}{na^2 \eta} \frac{\partial^2 R}{\partial e_y \partial i} \Big\} \Delta e_y + \left\{ \frac{\eta}{na^2} \frac{\partial^2 R}{\partial e_x \partial i} \right. \\
 & + \frac{e_x \csc^2 i}{na^2 \eta} \frac{\partial R}{\partial i} - \frac{e_x \cot i}{na^2 \eta} \frac{\partial^2 R}{\partial i^2} \Big\} \Delta i + \left\{ \frac{\eta}{na^2} \frac{\partial^2 R}{\partial e_x \partial \Omega} - \frac{e_x \cot i}{na^2 \eta} \frac{\partial^2 R}{\partial i \partial \Omega} \right\} \Delta \Omega \\
 \Delta \delta i \approx & \left\{ \frac{\cot i}{na^2 \eta} \left( e_x \frac{\partial^2 R}{\partial a \partial e_y} - e_y \frac{\partial^2 R}{\partial a \partial e_x} \right) - \frac{\csc i}{na^2 \eta} \frac{\partial^2 R}{\partial a \partial \Omega} - \frac{2 d \delta i}{a dt} \right\} \cdot \Delta a \\
 & + \left\{ \frac{e_x \cot i}{na^2 \eta^3} \left( e_x \frac{\partial R}{\partial e_y} - e_y \frac{\partial R}{\partial e_x} \right) + \frac{\cot i}{na^2 \eta} \left( \frac{\partial R}{\partial e_y} + e_x \frac{\partial^2 R}{\partial e_x \partial e_y} - e_y \frac{\partial^2 R}{\partial e_x^2} \right) \right. \\
 & - \frac{e_x \csc i}{na^2 \eta^3} \frac{\partial R}{\partial \Omega} - \frac{\csc i}{na^2 \eta} \frac{\partial^2 R}{\partial e_x \partial \Omega} \Big\} \cdot \Delta e_x + \left\{ \frac{e_y \cot i}{na^2 \eta^3} \left( e_x \frac{\partial R}{\partial e_y} - e_y \frac{\partial R}{\partial e_x} \right) \right. \\
 & + \frac{\cot i}{na^2 \eta} \left( e_x \frac{\partial^2 R}{\partial e_y^2} - \frac{\partial R}{\partial e_x} - e_y \frac{\partial^2 R}{\partial e_x \partial e_y} \right) - \frac{e_y \csc i}{na^2 \eta^3} \frac{\partial R}{\partial \Omega} - \frac{\csc i}{na^2 \eta} \frac{\partial^2 R}{\partial e_y \partial \Omega} \Big\} \\
 & \times \Delta e_y + \left\{ -\frac{\csc^2 i}{na^2 \eta} \left( e_x \frac{\partial R}{\partial e_y} - e_y \frac{\partial R}{\partial e_x} \right) + \frac{\cot i}{na^2 \eta} \left( e_x \frac{\partial^2 R}{\partial e_y \partial i} - e_y \frac{\partial^2 R}{\partial e_x \partial i} \right) \right. \\
 & + \frac{\csc i \cot i}{na^2 \eta} \frac{\partial R}{\partial \Omega} - \frac{\csc i}{na^2 \eta} \frac{\partial^2 R}{\partial i \partial \Omega} \Big\} \cdot \Delta i + \left\{ \frac{\cot i}{na^2 \eta} \left( e_x \frac{\partial^2 R}{\partial e_y \partial \Omega} - e_y \frac{\partial^2 R}{\partial e_x \partial \Omega} \right) \right. \\
 & \left. - \frac{\csc i}{na^2 \eta} \frac{\partial^2 R}{\partial \Omega^2} \right\} \cdot \Delta \Omega
 \end{aligned}$$

$$\Delta\delta\dot{\Omega} \approx \frac{\csc i}{na^2\eta} \left\{ \left( \frac{\partial^2 R}{\partial a \partial i} - \frac{2}{a} \frac{\partial R}{\partial i} \right) \cdot \Delta a + \left( \frac{e_x}{\eta^2} \frac{\partial R}{\partial i} + \frac{\partial^2 R}{\partial e_x \partial i} \right) \cdot \Delta e_x + \left( \frac{e_y}{\eta^2} \frac{\partial R}{\partial i} + \frac{\partial^2 R}{\partial e_y \partial i} \right) \cdot \Delta e_y + \left( \frac{\partial^2 R}{\partial i^2} - \cot i \frac{\partial R}{\partial i} \right) \cdot \Delta i + \frac{\partial^2 R}{\partial i \partial \Omega} \cdot \Delta \Omega \right\}.$$

The explicit formulas for the first and second partial derivatives of the disturbing potential  $R$  are provided in the Electronic Supplement.

The relations in Eq. (5) are applied to obtain from the above formulas the rates of the perturbations in ROEs. In particular, the change in the second component of the relative inclination vector corresponding to the time span  $\Delta t$  can be derived following

$$\Delta\delta i_{y,\text{Sun/Moon}} = \Delta(\sin i \Delta\Omega) \approx \left( \cos i \frac{di}{dt} \Delta\Omega + \sin i \Delta\delta\dot{\Omega} \right) \Delta t,$$

Analogously, for the relative mean longitude

$$\Delta\delta\lambda_{\text{Sun/Moon}} = \Delta(\Delta u + \cos i \Delta\Omega) \approx \left( \Delta\delta\dot{u} - \sin i \frac{di}{dt} \Delta\Omega + \cos i \Delta\delta\dot{\Omega} \right) \Delta t,$$

while the change in the remaining ROEs is estimated according to

$$\begin{aligned} \Delta\delta e_{x,\text{Sun/Moon}} &\approx \Delta\delta\dot{e}_x \cdot \Delta t, & \Delta\delta e_{y,\text{Sun/Moon}} &\approx \Delta\delta\dot{e}_y \cdot \Delta t, \\ \Delta\delta i_{x,\text{Sun/Moon}} &\approx \Delta\delta\dot{i} \cdot \Delta t. \end{aligned}$$

### 4 Numerical validation

In this section, several test runs covering some typical scenarios related to on-orbit servicing are performed, giving an insight into the accuracy of the extended model and the magnitudes of the involved perturbations. In the following, the model of  $J_2$ -perturbed relative motion from Gaias et al. (2015) is referred to as  $\text{RMM}_{\text{HCW}+J_2}$ . The extension of  $\text{RMM}_{\text{HCW}+J_2}$  containing SRP perturbations is denoted by  $\text{RMM}_{\text{HCW}+J_2+\text{SRP}}$ , while the complete relative motion model is denoted by  $\text{RMM}_{\text{HCW}+J_2+\text{SRP}+3\text{B}}$ .

Table 1 provides the parameters adopted for the two hypothetical spacecraft. As the Servicer might be carrying additional fuel and/or replacement units for the Client spacecraft, it was assumed that the mass of the Servicer is 70 % higher than the Clients mass.

Three Initial Formation Geometries (IFGs) were selected for evaluation of the extended model performance. The initial osculating elements of the Servicer and the Client are summarized in the upper part of Table 2, while the corresponding initial ROEs are provided in the lower part of Table 2. The initial osculating elements of the Client spacecraft are assumed to be the same for the three initial formation geometries, i.e. only the initial osculating elements of the Servicer vary to allow different formation configurations. Moreover, selected initial formation geometries are tagged with three different epochs to illustrate seasonal effects related to the motion of the Moon around the Earth and the motion of the Earth around the Sun.

**Table 1** Spacecraft parameters

	$C_R$ (-)	$A_R$ (m <sup>2</sup> )	Mass (kg)
Servicer	1.2	40.0	1700
Client	1.2	40.0	1000

**Table 2** Initial conditions of absolute and relative orbits

		$a^0$ (km)	$e^0$ (-)	$i^0$ (°)	$\Omega^0$ (°)	$\omega^0$ (°)	$M^0$ (°)
<i>Initial osculating elements of the Client and the Servicer</i>							
	Client	42166.0085	1.236e-4	4.349e-2	270.7	160.0	148.5
Dec. 23	Servicer	42165.9785	1.209e-4	4.335e-2	270.6	157.1	151.6
June 30	Servicer	42166.0085	1.258e-4	4.361e-2	270.7	160.4	148.2
May 10	Servicer	42166.0085	1.241e-4	4.349e-2	270.9	159.4	149.0
		$a\delta a^0$ (m)	$a\delta\lambda^0$ (m)	$a\delta e_x^0$ (m)	$a\delta e_y^0$ (m)	$a\delta i_x^0$ (m)	$a\delta i_y^0$ (m)
<i>Initial formation geometries</i>							
IFG1	Dec. 23	-30.0	-3500.0	200.0	200.0	-100.0	-100.0
IFG2	June 30	0.0	0.0	-100.0	0.0	90.0	0.0
IFG3	May 10	0.0	0.0	0.0	60.0	0.0	70.0

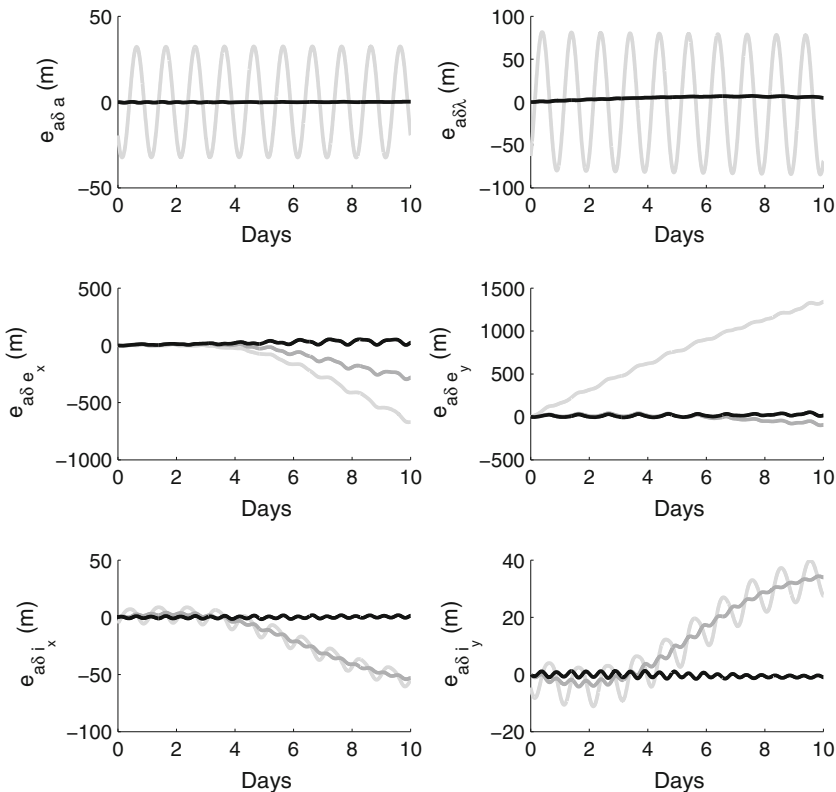


**Fig. 1** Errors for IFG1 of different RMM configurations: previously existing RMM<sub>HCW+J<sub>2</sub></sub> (light grey), extension RMM<sub>HCW+J<sub>2</sub>+SRP</sub> (dark grey), complete final RMM<sub>HCW+J<sub>2</sub>+SRP+3B</sub> (black)

In the context of On-Orbit Servicing, IFG1 initializes an approach trajectory with a constant relative drift rate of about 280m per orbit starting from a hold point 3.5km away in anti-flight direction. For the sake of formations’ safety, anti-parallel relative eccentricity and

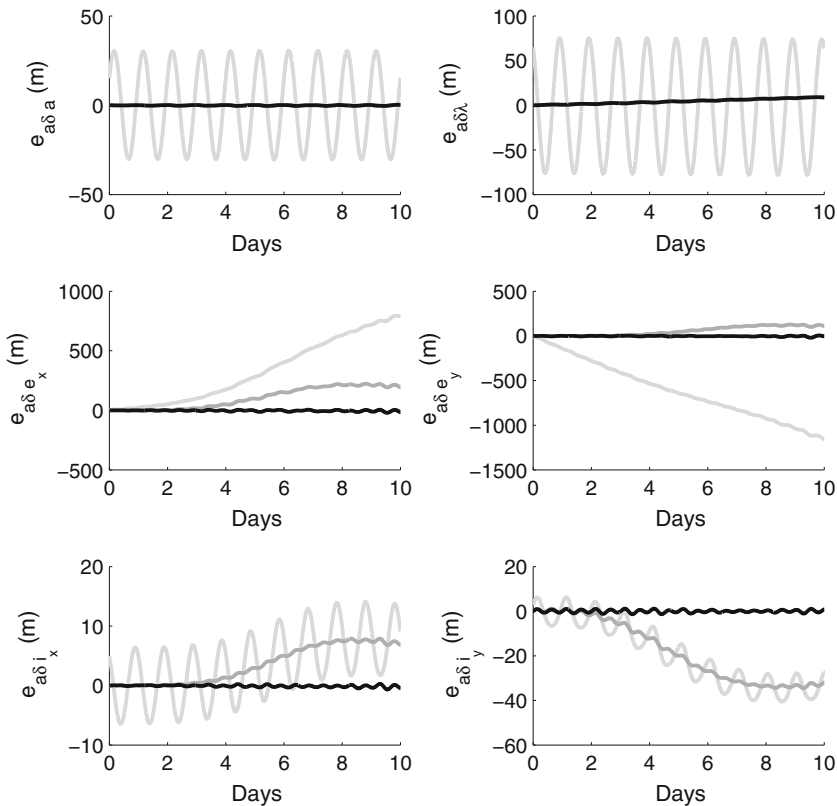


**Fig. 2** Errors for IFG2 of different RMM configurations: previously existing RMM<sub>HCW+J<sub>2</sub></sub> (light grey), extension RMM<sub>HCW+J<sub>2</sub>+SRP</sub> (dark grey), complete final RMM<sub>HCW+J<sub>2</sub>+SRP+3B</sub> (black)

inclination vectors are selected so that the Servicer performs additionally a Client-centered elliptical motion in the plane perpendicular to the flight direction. In the presence of large along-track errors, this so-called eccentricity and inclination vector separation allows a passive collision risk prevention (Montenbruck et al. 2006). The second case, IFG2, represents a bounded relative orbit with horizontal anti-parallel relative eccentricity and inclination vectors, whereas IFG3 features vertical parallel  $ade$  and  $adi$  of somewhat smaller magnitude. The last two relative orbits represent the case, where the Servicer performs a Client-centered motion in both the orbital plane and the plane orthogonal to the flight direction. Such a geometry could be used, for instance, for inspection purposes to establish the cause of targets malfunctioning or for identifying a suitable docking area.

For the performance evaluation of the extended RMM, a numerical integration with a full force model – including Earth gravity field of degree and order 10, SRP, gravitational potential of the Sun and the Moon, and the solid Earth tides – was performed for the absolute orbits of the Client and the Servicer. At this point, the GRACE gravity model GGM01S as implemented in the flight dynamics library routines of GSOC/DLR was used, while the initial osculating elements as summarized in Table 2 provided the starting points of integration. Finally, a time-series of reference ROEs was built based on the two time-series of osculating elements obtained independently for the Client and the Servicer.

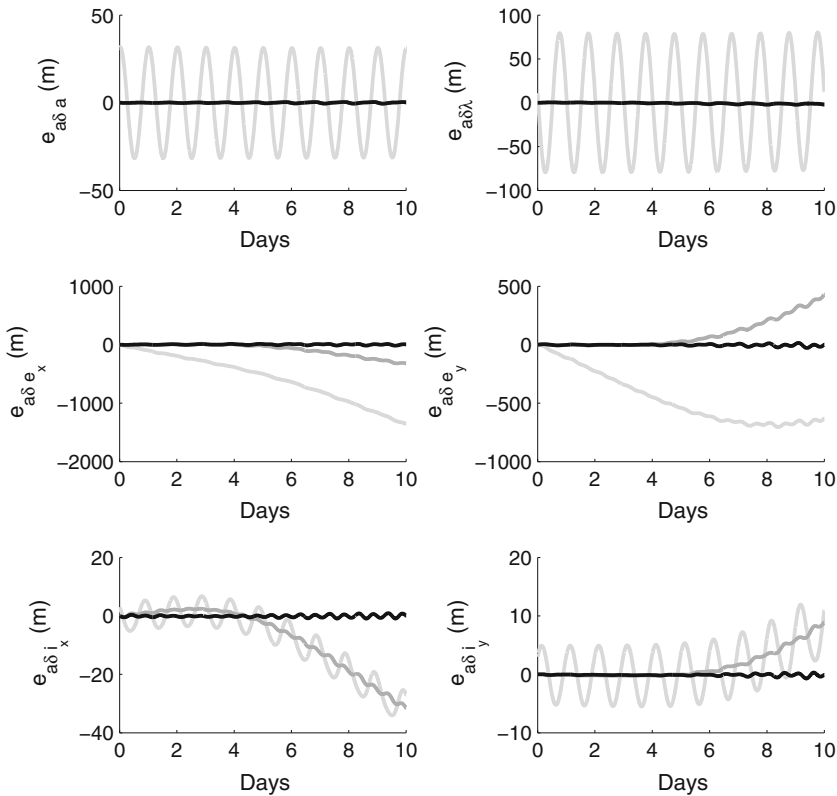


**Fig. 3** Errors for IFG3 of different RMM configurations: previously existing  $RMM_{HCW+J_2}$  (light grey), extension  $RMM_{HCW+J_2+SRP}$  (dark grey), complete final  $RMM_{HCW+J_2+SRP+3B}$  (black)

Figures 1, 2 and 3 show the errors of various RMM configurations calculated as differences between the modeled and the reference time-series of ROEs for the three selected initial formation geometries. Having a look at the general character of the SRP and third-body perturbations, it can be noticed that SRP results in short-periodic perturbations in  $\delta a$ ,  $\delta \lambda$ ,  $\delta i_x$  and  $\delta i_y$ . At the same time, in the relative eccentricity components  $\delta e_x$  and  $\delta e_y$ , the effects of SRP are mainly of long-periodic nature. On the other hand, the third-body perturbations produce significant drifts both in the relative eccentricity and in the relative inclination components, whereas their short-periodic effects are less prominent. As Figs. 1, 2 and 3 demonstrate, the complete extended model  $RMM_{HCW+J_2+SRP+3B}$  accounts for all the major short- and long-periodic effects of SRP as well as for the drifts in the relative eccentricity and inclination vector components due to the third-body perturbations.

It is important to note that the former model  $RMM_{HCW+J_2}$  requires special initial conditions to avoid non-zero error offsets. Since the periodic perturbations due to SRP make the affected orbital elements increase along one half-orbit, and decrease along the other half-orbit, the instantaneous initial relative element will be either higher or lower than the average value, depending on where the point of initialization is located along the orbit. In order to have a zero-mean error with the former model, an averaging of the initial osculating elements over the periodic effects of SRP should be performed before they are provided as input for  $RMM_{HCW+J_2}$ . The general problem of choosing the correct initial conditions when

using  $\text{RMM}_{\text{HCW}+J_2}$  was addressed in [Gaias et al. \(2015\)](#) on the example of the  $J_2$  periodic perturbations in LEO formations.

Contrary to that, the extended RMM can account for the varying SRP effects from  $t$  to  $t + \Delta t$  along the satellite orbit, thus, no averaging of the initial conditions is required prior to ROEs initialization for  $\text{RMM}_{\text{HCW}+J_2+\text{SRP}}$  and  $\text{RMM}_{\text{HCW}+J_2+\text{SRP}+3B}$ , i.e., the osculating orbital elements can be used directly as they would come from absolute orbit determination (in a real scenario).

## 5 Conclusions

This work addresses a novel topic of formation dynamics in near-geostationary orbit. For the first time, a dedicated relative motion model is developed for two spacecraft located in the geostationary ring. An already existing model for LEO satellite formations including secular perturbations due to Earth equatorial bulge constitutes the foundation for the new extended relative motion model. In the context of on-orbit servicing and formation flying in GEO, long revolution periods lead to extensive timely duration of any proximity operation requiring a certain number of relative orbits. Thus, various secular and long-periodic perturbations, which are negligible in LEO, have a major influence on the evolution of the relative geometry in GEO. In particular, the new model addresses perturbations of the relative orbit due to the solar radiation pressure, as well as secular and long-periodic perturbations due to third-body gravitational potential of the Sun and the Moon. The modeling of the differential solar radiation pressure is based on the difference in area-to-mass ratios of the two spacecraft, while the developments of the third-body perturbations are based on the single-averaged disturbing potential of [Kozai \(1973\)](#). Explicit expressions are provided describing the evolution of ROEs from epoch  $t$  to the next epoch  $t + \Delta t$ , allowing a step-wise prediction of the relative orbit over time.

A simulation encompassing three typical formation geometries is performed for validation of the new extended model against the reference relative orbital elements build from numerically integrated absolute orbits of two hypothetical spacecraft. The results of the validation prove that all secular and long-periodic error drifts in relative orbital elements result eliminated, and, therefore, the new model achieves high accuracy even on the tenth day of simulation time. Thus, the developed relative motion model can be incorporated into guidance, navigation and control algorithms on-board the Servicer spacecraft for support of autonomous relative orbit determination and fuel-efficient formation keeping maneuver planning up to several weeks in advance. The suggested relative motion model contributes to the general understanding of how the solar radiation pressure and the third-body gravitational potential might affect relative motion and, in particular, gives an insight into formation dynamics in near-geostationary orbit for the potential use of future on-orbit servicing missions.

**Acknowledgments** The author is grateful to Dr. R. Kahle for the many helpful discussions, as well as to Dr. G. Gaias for the valuable suggestions that improved the quality of the paper. The author also thanks the anonymous reviewers for the careful reading of the paper and insightful comments.

## References

Aksnes, K.: Short-period and long-period perturbations of a spherical satellite due to direct solar radiation. *Celest. Mech.* **13**, 89–104 (1976)

- Ardaens, J.-S., D'Amico, S., Fischer, D.: Early flight results from the TanDEM-X autonomous formation flying system. In: 4th International Conference on Spacecraft Formation Flying Missions and Technologies (SFFMT), St-Hubert, Quebec (2011)
- Ardaens, J.-S., Kahle, R., Schulze, D.: In-flight performance validation of the TanDEM-X autonomous formation flying system. In: 5th International Conference on Spacecraft Formation Flying Missions and Technologies (SFFMT), Munich, Germany (2013)
- Bryant, R. W.: The effect of solar radiation pressure on the motion of an artificial satellite. NASA Technical Note D-1063 (1961)
- Caswell, D. et al.: ConeXpress orbital life extension vehicle—a commercial service for communications satellites. *ESA Bull.* **127**, 54–61 (2006)
- Clohesy, W.H., Wiltshire, R.S.: Terminal guidance system for satellite rendezvous. *J. Aerosp. Sci.* **27**(9), 653–658 (1960)
- D'Amico, S.: Autonomous formation flying in low-Earth orbit, PhD Thesis, Technical University of Delft (2010)
- D'Amico, S., Ardaens, J.-S., Larsson, R.: Spaceborne autonomous formation-flying experiment on the PRISMA mission. *J. Guid. Control Dyn.* **35**(3), 834–850 (2012)
- D'Amico, S., Ardaens, J.-S., Gaias, G., Benninghoff, H., Schlepp, B., Jørgensen, J.L.: Noncooperative rendezvous using angles-only optical navigation: system design and flight results. *J. Guid. Control Dyn.* **36**(6), 1576–1595 (2013)
- Eckstein, M. C., Rajasingh, C. K., and Blumer, P.: Colocation strategy and collision avoidance for the geostationary satellites at 19 degrees West. In: CNES International Symposium on Space Dynamics (1989)
- Gaias, G., D'Amico, S., Ardaens, J.-S.: Angles-only navigation to a noncooperative satellite using relative orbital elements. *J. Guid. Control Dyn.* **37**(2), 439–451 (2014)
- Gaias, G., Ardaens, J.-S., D'Amico, S.: The autonomous vision approach navigation and target identification (AVANTI) experiment: objectives and design. In: 9th International ESA Conference on Guidance, Navigation & Control Systems, Porto, Portugal (2014)
- Gaias, G., Ardaens, J.-S., Montenbruck, O.: Model of  $J_2$  perturbed relative motion with time-varying differential drag. *Celest. Mech. Dyn. Astron.* **123**(4), 411–433 (2015)
- Giacaglia, G.E.O.: Lunar perturbations of artificial satellites of the Earth. *Celest. Mech.* **9**, 239–267 (1974)
- Härtling, A., Rajasingh, C.K., Eckstein, M.C., Leibold, A.F., and Srinivasamurthy, K.N.: On the collision hazard of collocated geostationary satellites. *AIAA/AAS Astrodyn. Conf. AIAA Pap.*, 1988–4239 (1988)
- Kaiser, C., Sjöberg, F., Delcura, J.M., Eilertsen, B.: SMART-OLEV—an orbital life extension vehicle for servicing commercial spacecrafts in GEO. *Acta Astronaut.* **63**(1–4), 400–410 (2008)
- Kaula, W.M.: Development of the lunar and solar disturbing functions for a close satellite. *Astronom. J.* **67**, 300–303 (1962)
- Kozai, Y.: Effects of solar radiation pressure on the motion of an artificial satellite. *Smithson. Contrib. Astrophys.* **6**, 109 (1963)
- Kozai, Y.: A new method to compute lunisolar perturbations in satellite motions. *Smithsonian Astrophysical Observatory Special Report* 349 (1973)
- Montenbruck, O., Gill, E.: *Satellite Orbits: Models Methods and Applications*. Springer, Heidelberg (2000)
- Montenbruck, O., Kirschner, M., D'Amico, S., Bettadpur, S.: E/I-vector separation for safe switching of the GRACE formation. *Aerosp. Sci. Technol.* **10**(7), 628–635 (2006)
- Prado, A.F.B.A.: Third-body perturbation in orbits around natural satellites. *J. Guid. Control Dyn.* **26**, 33–40 (2003)
- Roscoe, C.W.R., Vadali, S.R., Alfriend, K.T.: Third-body perturbation effects on satellite formations. *Adv. Astronaut. Sci.* **147**, 483–502 (2013)
- Ustinov, B.A.: Motion of satellites along low-eccentricity orbits in a noncentral terrestrial gravitational field. *Cosm. Res.* **5**, 159 (1967)
- Wnuk, E., Golebiewska, J.: The relative motion of Earth orbiting satellites. *Celest. Mech. Dyn. Astron.* **91**, 373–389 (2005)